Using cosmic-ray hodoscope data to validate the misalignment model of small-strip thin gap chambers for the ATLAS new small wheels

Lia Formenti

Department of Physics
McGill University, Montreal
August, 2021

A thesis submitted to
McGill University
in partial fulfillment of the
requirements of the degree of
Master of Science

Table of Contents

Abstract

ATLAS is a multi-purpose particle detector system designed to capture the outcome of proton-proton collisions at the Large Hadron Collider (LHC) at CERN. The innermost end-caps of the ATLAS muon spectrometer consist of two wheels of muon detectors that must be replaced to improve the angular resolution of tracks for precision muon momentum reconstruction in the next phase of LHC operation. The New Small Wheels (NSWs) will be covered with two detector types that must trigger on and track outgoing particles - one type is small-strip thin gap chambers (sTGCs). Canada is responsible for one quarter of the required sTGCs. At McGill University, modules with four layers of sTGCs (called quadruplets) are characterized using a cosmic ray hodoscope before being sent to CERN for further testing and integration into the wheels. Quadruplets must be able to reconstruct particle tracks with 1 mrad angular resolution. Misalignments between sTGC layers must be corrected for to achieve this goal. The charge profile left by an x-ray gun and coordinate measuring machine (CMM) measurements of quadruplet layers are being used to define these parameters. Work on using cosmic ray data to validate misalignment parameters derived using the above-mentioned methods will be presented.

Résumé

C'est le résumé.

Ad eros odio amet et nisl in nostrud consequat iusto eum suscipit autem vero enim dolore exerci, ut. Esse ex, magna in facilisis duis amet feugait augue accumsan zzril. Lobortis aliquip dignissim at, in molestie nibh, vulputate feugait nibh luptatum ea delenit nostrud dolore minim veniam odio. Euismod delenit nulla accumsan eum vero ullamcorper eum ad velit veniam. Quis, exerci ea feugiat nulla molestie, veniam nonummy nulla. Elit tincidunt, consectetuer dolore nulla ipsum commodo, ut, at qui blandit suscipit accumsan feugiat vel praesent.

Dolor zzril wisi quis consequat in autem praesent dignissim, sit vel aliquam at te, vero. Duis molestie consequat eros tation facilisi diam dolor augue. Dolore dolor in facilisis et facilisi et adipiscing suscipit eu iusto praesent enim, euismod consectetuer feugait duis vulputate.

Acknowledgements

Something along the lines of . . . I would like to thank all the little people who made this thesis possible.

Contribution of authors

Something along the lines of . . . I hereby declare that I am the sole author of this thesis. This is a true copy of the thesis, including any required final revisions, as accepted by my examiners.

Chapter 1

Using cosmic muon data for alignment studies

1.1 Measuring alignment using cosmics data

Misalignments can be modeled as passive transformations. Ideally, a misalignment model would be chosen and the parameters (for example, a global offset and rotation for each layer) calculated. To understand the potential of cosmic muon data, it is useful to define a local offset. For each area of a strip layer, the local offset is the offset of the strip pattern in that area with respect to the nominal geometry. Local offsets systematically change the strip that is hit by a muon passing through the area. The `tgc_analysis/CosmicsAnalysis` software assumes the nominal geometry, so the recorded muon y-position ($y_{cluster}$) is shifted opposite to the local offset (d_{local}),

$$y_{cluster} = y_{nom} - d_{local},\tag{1.1}$$

where y_{nom} is the position of the muon that would have been recorded if there was no local offset. Equation 1.1 ignores other factors that could affect the cluster position (like resolution). The local offset is unknown and there is no external reference to measure y_{nom}. Therefore, only relative alignment parameters can be extracted.

The minimal relative coordinate system uses two reference or fixed layers [1]. The hits on the two fixed layers were used to create tracks that can be interpolated or extrapolated (polated) to the other two layers. The residual of track i, Δ_i is defined as,

$$\Delta_i = y_{i,hit} - y_{i,track},\tag{1.2}$$

where $y_{i,hit}$ is the recorded hit position and $y_{i,track}$ is the polated track position built from hits on the two reference layers. Track residuals are affected by the local offset in the area of each layer's hit. As an example, in figure 1.1, the residual on layer 2 perhaps indicates that layer 2 is offset with respect to layers 1 and 4 in the area of the track. Of course, a single track residual says nothing of the real relative local offset because of the limited spatial resolution of the detectors and fake tracks caused by noise or delta rays. However, the mean of residuals for all tracks in a region will be shifted systematically by the local offsets between layers [1]. For a perfectly aligned quadruplet, the mean of residuals should be zero in all regions and for all reference frames, unlike the example regions shown in figure 1.2.

The residual distributions were wider for tracking combinations where the extrapolation lever arm was largest. In general, residual means calculated with geometrically less favourable tracking combinations have larger statistical and systematic uncertainties. The bin size of 200 μm for the distributions shown in figure 1.2 was chosen based on the uncertainty on residuals calculated from tracks on layer 4 (1) built from hits on layers 1 and 2 (3 and 4) given a cluster y-position uncertainty of 60 μm (A), since these tracks yield residuals with the largest uncertainties.

A gaussian fit was used to extract the mean of the residual distributions. Theoretically, a double gaussian distribution is more apt, but for this analysis the gaussian fit was sufficient, as discussed in appendix C.1.

The motivation for the area of the region of interest will be discussed in CHAPTER 5, COMPARISON (ADD IN REF ONCE CREATED).

It is only possible to calculate relative local offsets with csomics data because there was no external reference which positions on all layers could be measured with respect to. As an example, in figure 1.1, the residual on layer 2 could be caused by layer 2 being misaligned from nominal, but it could also be caused by layers 1 and 4 being misaligned from nominal while layer 2 is in its expected position! Any number of combinations of local offsets on layers 1, 2 and 4 could produce the residual on layer 2. Nonetheless, the value of relative local offset measurements will be shown and discussed throughout this work.

1.2   Visualizing relative misalignments between layers

The mean of residuals was extracted for regions across entire quadruplet layers for every tracking combination to get a picture of the relative misalignments between layers.

Figure 1.3, contains the mean of residuals on layers 2 and 4 with tracking reference layers 1 and 3. Many of the residual means are non-zero, indicating that there are local relative
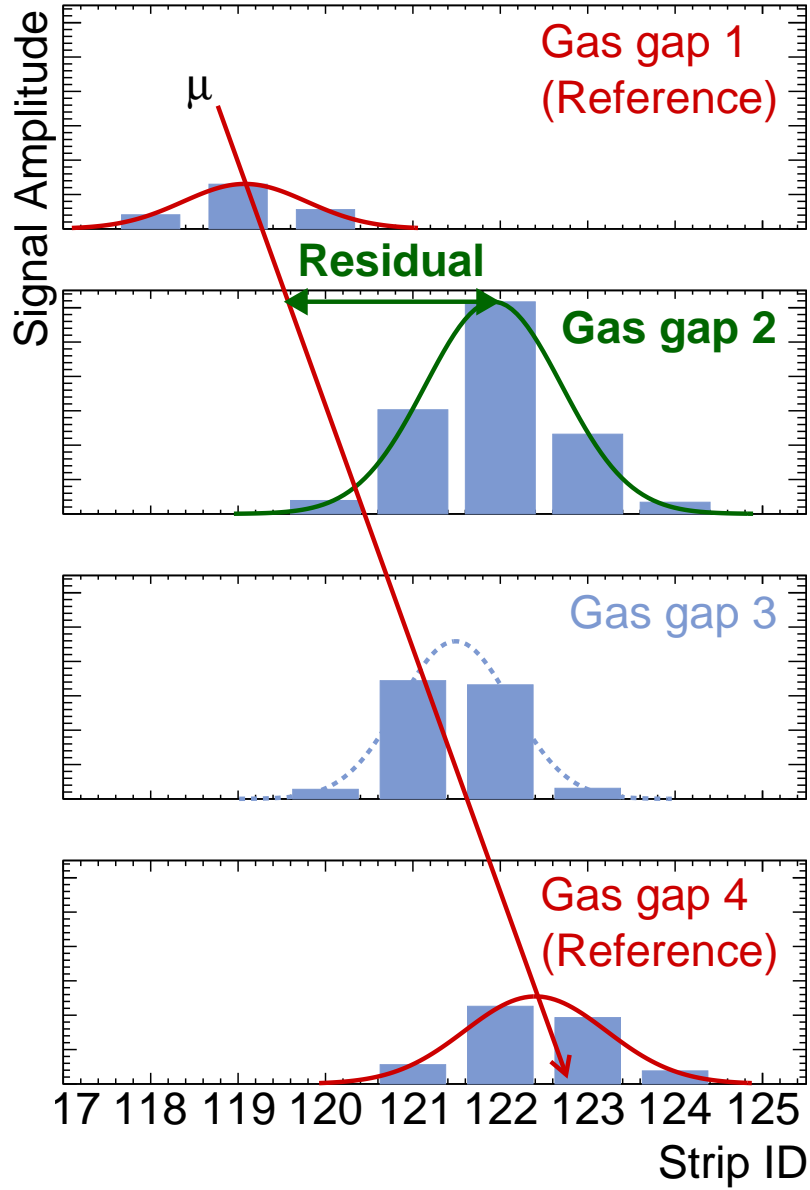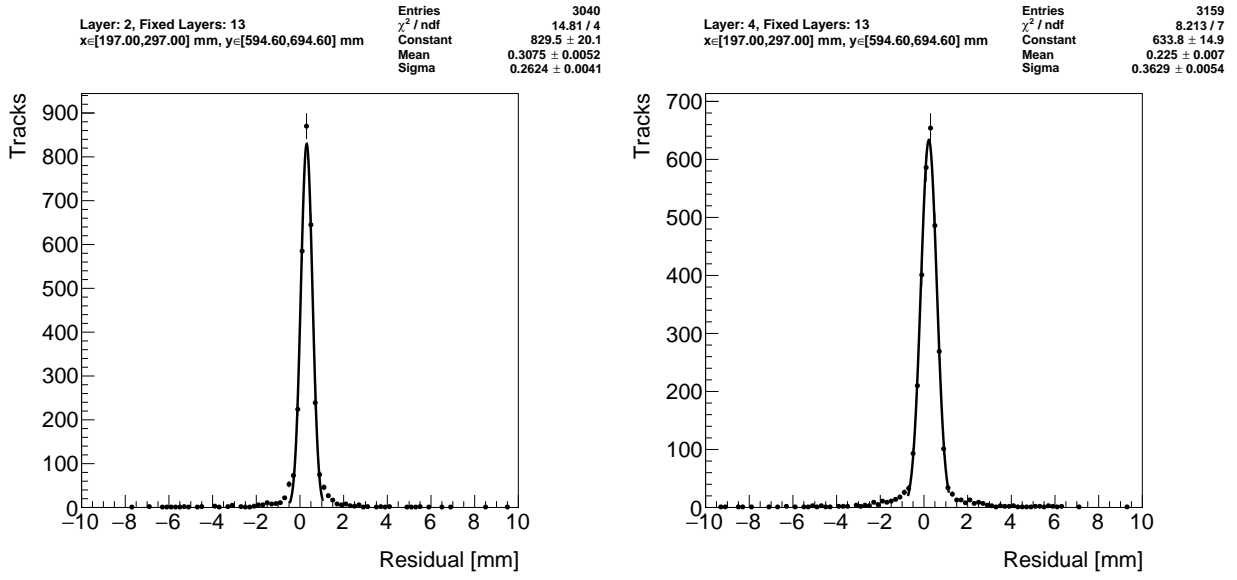
Figure 1.1: Representation of a muon event recorded by an sTGC. The clusters are fit with a Gaussian and the mean is taken as the hit position. A track is built from the chosen reference layers, 1 and 4, and the residual calculated on layer 2. The clusters come from a real muon event, but their positions were modified to highlight the idea of residuals.

		Entries	3040
Layer: 2, Fixed Layers: 13		χ^2 / ndf	14.81 / 4
x∈[197.00,297.00] mm, y∈[594.60,694.60] mm		Constant	829.5 ± 20.1
		Mean	0.3075 ± 0.0052
		Sigma	0.2624 ± 0.0041

|		Entries	3159
Layer: 4, Fixed Layers: 13		χ^2 / ndf	8.213 / 7
x∈[197.00,297.00] mm, y∈[594.60,694.60] mm		Constant	633.8 ± 14.9
		Mean	0.225 ± 0.007
		Sigma	0.3629 ± 0.0054

(a) Tracks on layer 2, reference layers 1 and 3.　　(b) Tracks on layer 4, reference layers 1 and 2.

Figure 1.2: Residual distribution in the region $x \in [197, 297]$, $y \in [594.6, 694.6]\,mm$ (100 mm by 100 mm area) for two different tracking combinations.
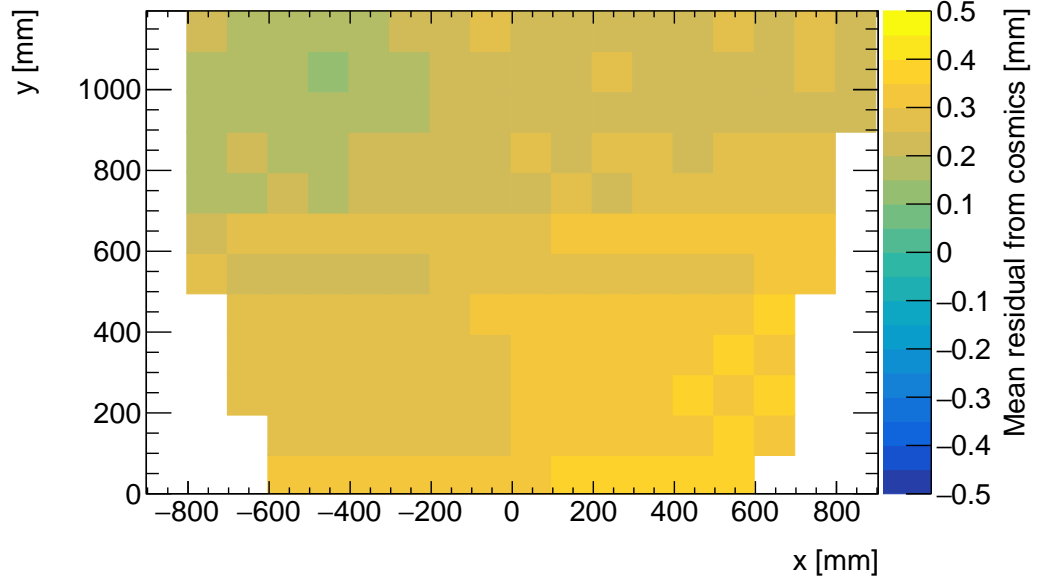
(a) Mean of residuals for tracks on layer 2, reference layers 1 and 3.
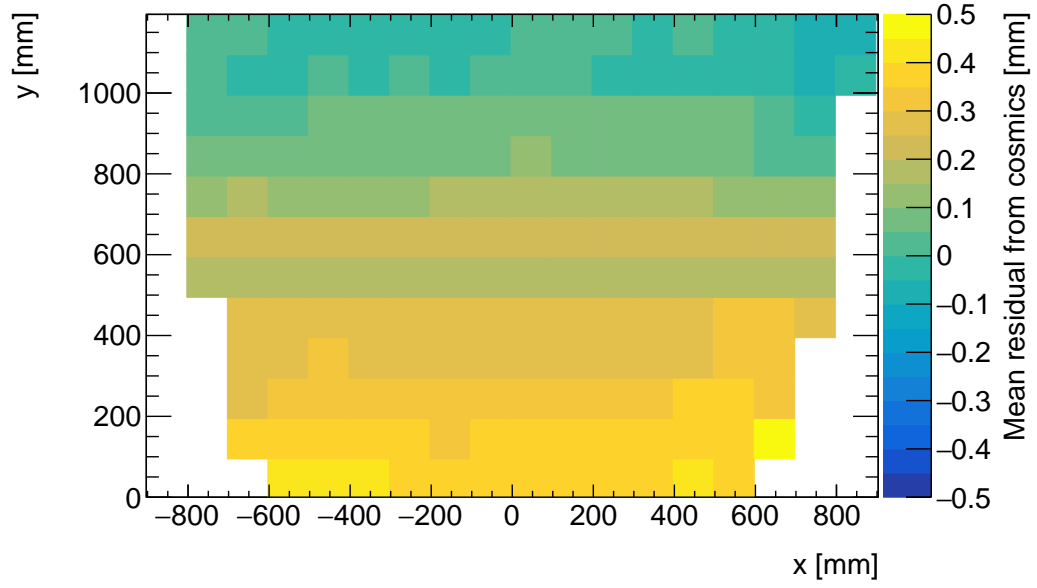
(b) Mean of residuals for tracks on layer 4, reference layers 1 and 3.

Figure 1.3: Mean of residuals in each 100 mm by 100 mm bin over the area of the quad layer.

misalignments. Given that the residual mean changes with x in figure 1.3a, there is likely a rotation of layer 2 with respect to layers 1 and 3, combined with an offset of the entire layer. For layer 4 in figure 1.3b, perhaps there is a scaling [2] of the strip pattern with respect to layers 1 and 3. The interpretation of the patterns in the residual means depends on the choice of misalignment model.

Work on characterizing relative misalignments between quadruplet layers in ongoing [3], (Can I cite John's thesis-in-progress?) but what is required are the absolute strip positions with respect to their nominal position in the ATLAS analysis coordinate system to be input into Athena(?). Somehow, absolute misalignment parameters must be derived to create a model of absolute strip positions - which is not possible with the cosmics dataset. Absolute local offset measurements were done by the so-called x-ray method, discussed in CHAPTER 4 X-RAY METHOD (REF ONCE CREATED). Given the degree of confidence in the local mean cosmic residual measurements detailed below, they were used to validate the absolute local offset measurements provided by the x-ray method (details to follow in CHAPTER 5 COMPARISON).

1.3   Systematic uncertainty

The statistical uncertainty on the local residual means was typically around 10 - 20 μm, and appendix B shows that the analysis was not statistically limited by the number of triggers collected for each quadruplet. The systematic uncertainties were more significant.

Systematic uncertainties were assigned per tracking combination as the RMS of the distribution of the difference in local residual means calculated each with a different analysis choice. For example, the RMS associated with fitting the local residual distributions with a Gaussian or double Gaussian is 25 μm for the geometrically least favourable tracking combinations and the distribution is shown in appendix C.1. For geometrically similar tracking combinations (like: tracks on layer 1 built from hits on layers 3 and 4, and tracks on layer 4 built from hits on layers 1 and 2), the systematic uncertainty was assigned as the average RMS for both.

Other choices were whether to use data collected at 2.9 kV or 3.1 kV; what cluster fitting algorithm to use; and whether or not to apply a differential non-linearity (DNL) correction to the cluster y-positions. A systematic uncertainty was assigned using the method above to account for the effect of each choice. The reasons for each choice are listed below.

Data taken at 3.1 kV was used over 2.9 kV because the strip and wire tracking efficiency increases with higher voltage [1] (appendix C.2).

Layer	Fixed layer 1	Fixed layer 2	C.1	C.2	C.3	C.5	Total
3	1	2	0.010	0.041	0.018	0.008	**0.047**
4	1	2	0.025	0.091	0.027	0.012	**0.098**
2	1	3	0.008	0.020	0.012	0.003	**0.025**
4	1	3	0.007	0.042	0.013	0.005	**0.044**
2	1	4	0.006	0.035	0.012	0.005	**0.038**
3	1	4	0.006	0.035	0.012	0.005	**0.038**
1	2	3	0.010	0.041	0.018	0.008	**0.047**
4	2	3	0.010	0.041	0.018	0.008	**0.047**
1	2	4	0.007	0.042	0.013	0.005	**0.044**
3	2	4	0.008	0.020	0.012	0.003	**0.025**
1	3	4	0.025	0.091	0.027	0.012	**0.098**
2	3	4	0.010	0.041	0.018	0.008	**0.047**

Table 1.1: Systematic uncertainty assigned for each analysis option, detailed in appendix C.

The `Minuit2` package [4] was used to fit clusters over Guo's method [5] because it provided automatic statistical uncertainty estimates and is the standard choice (appendix C.3).

The DNL correction was not applied because its effect on the residual means was negligible (appendix C.5).

A summary of the systematic uncertainties assigned for each tracking combination is given in table 1.1.

Given that the uncertainty in the cosmics residual means is lesser than or near to the order of the required position resolution of the sTGCs (100 μm [6] the cosmic residual means are relevant for characterizing misalignments.

References

[1] Benoit Lefebvre. *Characterization studies of small-strip Thin Gap Chambers for the ATLAS Upgrade*. PhD Dissertation, McGill University, Montreal, Canada, 2018.

[2] Evan Michael Carlson. *Results of the 2018 ATLAS sTGC test beam and internal strip alignment of sTGC detectors*. Thesis, University of Victoria, Victoria, Canada, 2019. Accepted: 2019-07-16T17:20:40Z.

[3] Xiao Zhao, Wenlong Li, Dengfeng Zhang, Changyu Li, Han Li, Shengquan Liu, Peng Miao, Yanyan Du, Yanyun Duan, and Chengguang Zhu. Cosmic test of sTGC detector prototype made in China for ATLAS experiment upgrade. *Nuclear Instruments and Methods in Physics Research Section A: Accelerators, Spectrometers, Detectors and Associated Equipment*, 927:257–261, May 2019.

[4] M. Hatlo, F. James, P. Mato, L. Moneta, M. Winkler, and A. Zsenei. Developments of mathematical software libraries for the LHC experiments. *IEEE Trans. Nucl. Sci.*, 52:2818–2822, 2005.

[5] Hongwei Guo. A Simple Algorithm for Fitting a Gaussian Function [DSP Tips and Tricks]. *IEEE Signal Processing Magazine*, 28(5):134–137, September 2011.

[6] T Kawamoto, S Vlachos, L Pontecorvo, J Dubbert, G Mikenberg, P Iengo, C Dallapiccola, C Amelung, L Levinson, R Richter, and D Lellouch. New Small Wheel Technical Design Report. Technical report, Jun 2013. ATLAS New Small Wheel Technical Design Report.

[7] B. Lefebvre. Precision survey of the readout strips of small-strip Thin Gap Chambers using X-rays for the muon spectrometer upgrade of the ATLAS experiment. *Journal of Instrumentation*, 15(07):C07013–C07013, July 2020.

[8] Ichita Endo, Tatsuo Kawamoto, Yoshinari Mizuno, Takashi Ohsugi, Takashi Taniguchi, and Tohru Takeshita. Systematic shifts of evaluated charge centroid for the cathode read-out multiwire proportional chamber. *Nuclear Instruments and Methods in Physics Research*, 188(1):51–58, September 1981.

[9] E. Perez Codina. Small-strip Thin Gap Chambers for the muon spectrometer upgrade of the ATLAS experiment. *Nuclear Instruments and Methods in Physics Research Section A: Accelerators, Spectrometers, Detectors and Associated Equipment*, 824:559–561, July 2016.

[10] S. Majewski, G. Charpak, A. Breskin, and G. Mikenberg. A thin multiwire chamber operating in the high multiplication mode. *Nuclear Instruments and Methods*, 217:265–271, 1983.

[11] Bernd Stelzer. The New Small Wheel Upgrade Project of the ATLAS Experiment. *Nuclear and Particle Physics Proceedings*, 273-275:1160–1165, April 2016.

[12] Angel Abusleme, Camille Bélanger-Champagne, Alain Bellerive, Yan Benhammou, James Botte, Hadar Cohen, Merlin Davies, Yanyan Du, Lea Gauthier, Thomas Koffas, Serguei Kuleshov, Benoit Lefebvre, Changyu Li, Nachman Lupu, Giora Mikenberg, Daniel Mori, Jean-Pierre Ochoa-Ricoux, Estel Perez Codina, Sebastien Rettie, Andree Robichaud-Véronneau, Rimsky Rojas, Meir Shoa, Vladimir Smakhtin, Bernd Stelzer, Oliver Stelzer-Chilton, Alam Toro, Heberth Torres, Pablo Ulloa, Brigitte Vachon, Gerardo Vasquez, Aleksander Vdovin, Simon Viel, Pablo Walker, Stephen Weber, and Chengguang Zhu. Performance of a Full-Size Small-Strip Thin Gap Chamber Prototype for the ATLAS New Small Wheel Muon Upgrade. *Nuclear Instruments and Methods in Physics Research Section A: Accelerators, Spectrometers, Detectors and Associated Equipment*, 817:85–92, May 2016. arXiv: 1509.06329.

[13] Fabio Sauli. Principles of operation of multiwire proportional and drift chambers. In *Cern Yellow Reports: Monographs*, page 92 p, Geneva, 1977. CERN, CERN. CERN, Geneva, 1975 - 1976.

[14] G Apollinari, I Bejar Alonso, O Bruning, P Fessia, M Lamont, L Rossi, and L Tavian. High-Luminosity Large Hadron Collider (HL-LHC) Technical Design Report V. 0.1. Technical report, CERN, Geneva, September 2017.

[15] L Evans and P Bryant. LHC Machine. *Journal of Instrumentation*, 3(S08001), 2008.

[16] ATLAS Collaboration. ATLAS Muon Spectrometer: Technical Design Report. Technical Report CERN-LHCC-97-022, CERN, Geneva, 1997.

[17] The ATLAS Collaboration. The ATLAS Experiment at the CERN Large Hadron Collider. *Journal of Instrumentation*, 3(08):S08003, 2008.

[18] Manfred Krammer. Upgrade Programs of the LHC Experiment, November 2017.

[19] The HL-LHC Project.

[20] S. Aefsky, C. Amelung, J. Bensinger, C. Blocker, A. Dushkin, M. Gardner, K. Hashemi, E. Henry, B. Kaplan, P. Keselman, M. Ketchum, U. Landgraf, A. Ostapchuk, J. Rothberg, A. Schricker, N. Skvorodnev, and H. Wellenstein. The Optical Alignment System of the ATLAS Muon Spectrometer Endcaps. *Journal of Instrumentation*, 3(11):P11005–P11005, November 2008. Publisher: IOP Publishing.

[21] Letter of Intent for the Phase-I Upgrade of the ATLAS Experiment. Technical report, CERN, Geneva, Nov 2011.

[22] John Townsend. *Electricity in gases*. Clarendon Press, Oxford, 1915.

APPENDICES

Appendix A

Uncertainty in cluster positions

A cluster is a series of contiguous strip channels on a layer with non-zero amplitude, all part of the same trigger and having the same event number [1]. Clusters result from the drift of ionization products generate in the ionization avalanche caused by a muon [22]. The peak-detector-output (PDO) of the signal on each strip of a cluster is fit with a Gaussian. The y-position of a particle as it passed through the layer is mean of the cluster, referred to here as the hit position.

The clusters were fit with Guo's method [5] and Minuit2 for ROOT [4]. The difference in cluster means between the two algorithms is shown in figure A.1.

The RMS of the distribution in figure A.1 is 57 μm, which is much larger than the statistical uncertainty in the mean for the Minuit2 algorithm, which peaks around 7 μm. An RMS of 60 μm is common for data taken with most quadruplets at 3.1 kV. Therefore, the uncertainty in the y-hit positions is assigned 60 μm.

The uncertainty assigned to the hit position affected the uncertainty in the extrapolated/interpolated position of the track, and in the residuals. The bin size of the residual distributions was set to 200 μm because that was the uncertainty in the residuals calculated from the tracks with the least favourable geometry (like tracks built from hits on layers 1 and 2 and extrapolated to layer 4).

The x position of the hit was taken to be the center of the wire group with the maximum peak detector output, since wire groups are much wider than the typical charge distribution spread. Assuming that the true x-position of the hit is uniformly distributed over the width of the wire group, the uncertainty in the x-position is given by $\frac{w}{\sqrt{(12)}}$, where w is the width
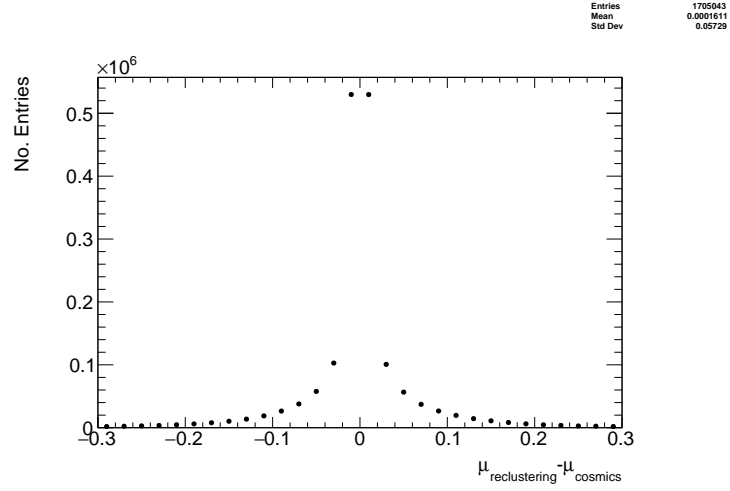
Figure A.1: The difference between cluster means calculated with Guo's method [5] in tgc_analysis/CosmicsAnalysis and Minuit2 for ROOT [4] in strip_position_analysis/ReClustering for data collected with QL2.P.8 at 3.1 kV.

of the wire group [13]. sTGC wire groups are 36 mm wide so the hit x-position uncertainty was 10 mm.

Appendix B

Study of cosmics for alignment analysis statistical uncertainty

Typically, one million triggers (cosmic muon events and noise) were collected for each Canadian quadruplet at McGill University, resulting in roughly half the number of viable tracks after cuts in `tgc_analysis/CosmicsAnalysis`. For QS3.P.18, 3.5 million triggers were collected. To gauge the sensitivity of the analysis to the available statistics, partitions of this data with each with a different number of triggers were analyzed separately. Ultimately, the quantity of interest was the gaussian mean of the residual distribution in regions of interest, so the peak in the distribution of the statistical uncertainty in the residual means for each area of interest for a specific tracking combination was used to gauge the quality of the analysis. How the peak in the residual mean uncertainty distribution changes with the number of triggers is shown in figure for tracks on layer 1 built from layers 3 and 4 B.1.

The uncertainty is already around 20 μm at 1 million triggers, suitable for distinguishing differences in offsets of order 50 μm as required. Although increased statistics could decrease the statistical uncertainty, it is not required for the goals of this analysis. Moreoever, the systematic uncertainty is around 50 μm and the systematic uncertainty on the x-ray residuals is 150 μm so the statistical uncertainty of 20 μm is nearly negligible.
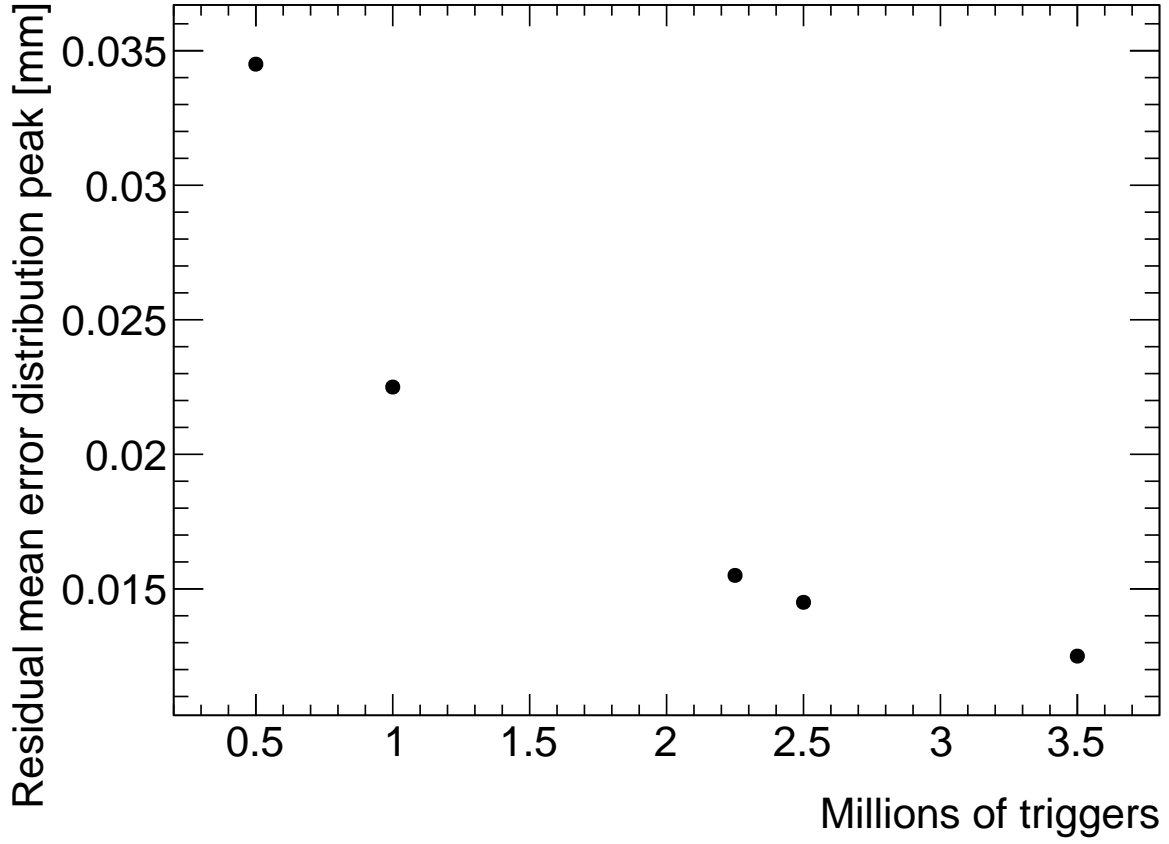
Figure B.1: How the peak of the distributions of uncertainties in the residual means in regions ofinterest for tracks on layer 1 built from layers 3 and 4 changed with the number of triggers used in the analysis. The distribution falls off as $\frac{1}{\sqrt{N}}$ as expected.

Appendix C

Study of systematic uncertainties when using cosmics data for alignment studies

C.1 Residual distribution fit function

The distribution of residuals should be modelled by a double gaussian fit[1]:

$$G(r) = A_s exp \left[\frac{-(r - \mu)^2}{2\sigma_s^2} \right] + A_b exp \left[\frac{-(r - \mu)^2}{2\sigma_b^2} \right] \tag{C.1}$$

where r is the residual, A is the gaussian amplitude, μ is the gaussian mean, σ is the gaussian sigma, and the subscripts s and b stand for signal and background respectively. One gaussian captures the real (signal) tracks and the other captures the tracks built from noise (background). The gaussian with the smaller width is identified as the signal.

A single gaussian fit failed less often than a double gaussian fit. The gaussian fits were performed by initially estimating the amplitude to be 100 tracks, the gaussian mean to be the histogram mean, and gaussian σ to be the RMS. The fit range was restricted to ± 1 RMS from the histogram mean. The modification helped the gaussian fit capture the signal peak. An example residual distribution is shown in figure C.1.

For all residual distributions in 100 mm by 100 mm bins on layer 4 built from hits on layers 1 and 2, the difference in gaussian and double gaussian means and σ's is shown in figure C.2.
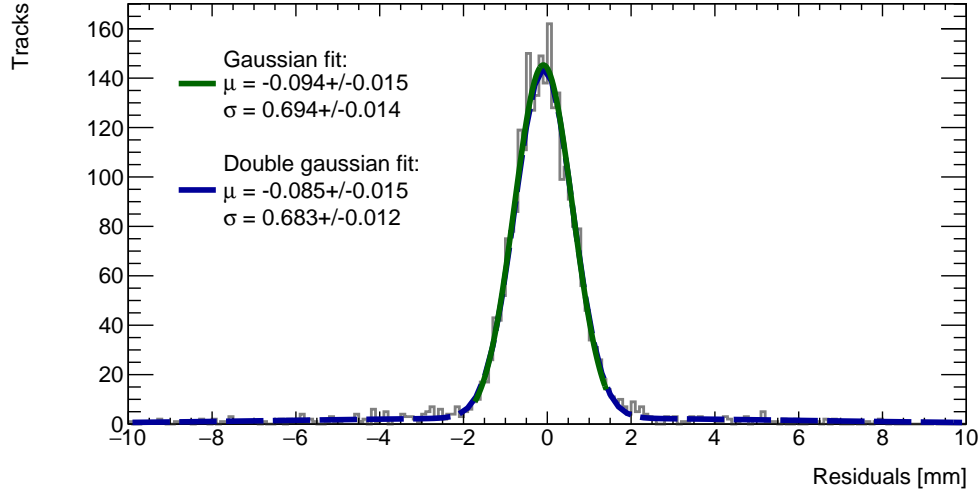
Figure C.1: Residual distribution for tracks on layer 4 built from hits on layers 1 and 2 for $x \in [-3.00, 97.00]$, $y \in [394.60, 494.60]$ mm for QL2.P.8 fit with a double gaussian and a single gaussian in a range of ± 1 RMS from the histogram mean.

Since the RMS of the residual mean differences distribution is less than $50\,\mu m$ the gaussian fit gave the same result within the required precision. Moreover, this is for the tracking combination with the worst extrapolation lever arm and the widest distribution of mean differences; the interpolation combinations have narrower distributions.

The gaussian σ should be larger than the double gaussian σ because the gaussian distribution includes the effect of the noise tracks with large residuals, while the double gaussian models signal and background residuals separately. For this analysis, only the residual mean was important, so the systematic overestimate of the signal σ in the gaussian fit shown on the right of figure C.2 was allowed.

C.2   Cosmic muon data collection voltage

Cosmic muon data was collected at 2.9 kV and 3.1 kV because although 2.9 kV is closer to the operating conditions the chambers will be subject to in ATLAS, the extra gain provided by operating at 3.1 kV increased the signal to noise ratio for pad signals. Also, the tracking efficiency was higher with data collected at 3.1 kV. The difference in gain affected the relative population of clusters of different sizes, which in turn affected the uncertainty in the strip hit
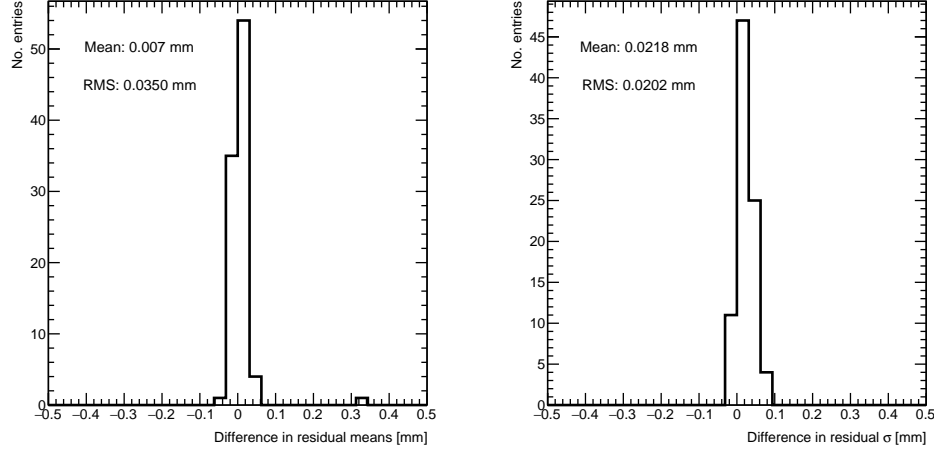
Figure C.2: Difference in residual distribution means and σ's for a gaussian and double gaussian fit, for all residual distributions in 100 mm by 100 mm bins on layer 4 built from hits on layers 1 and 2 for QL2.P.8.

positions on each layer, the uncertainty in the track positions and the residual distributions. The residual distributions for 3.1 kV data are narrower, as shown in figure C.3.

Neither dataset is better for calculating the mean of residuals in a given area, so a systematic uncertainty can be assigned based on the difference in residual means calculated for 2.9 kV and 3.1 kV data; namely, the systematic uncertainty was approximated as the RMS of the residual mean difference distribution. Data taken with QL2.P.8 was used to estimate the RMS, as in figure C.4a.

Tracks built from hits on layers 1 and 2 and extrapolated to layer 4 have the worst lever arm and hence the most uncertainty. The width of the distribution for geometrically favourable tracks are much narrower. The narrowest width of the residual mean difference distribution is for tracks on layer 2 built from hits on layers 1 and 3 (see figure C.4b).

Therefore, for each tracking combination, a systematic uncertainty equal to the RMS of the residual mean difference distribution was assigned.
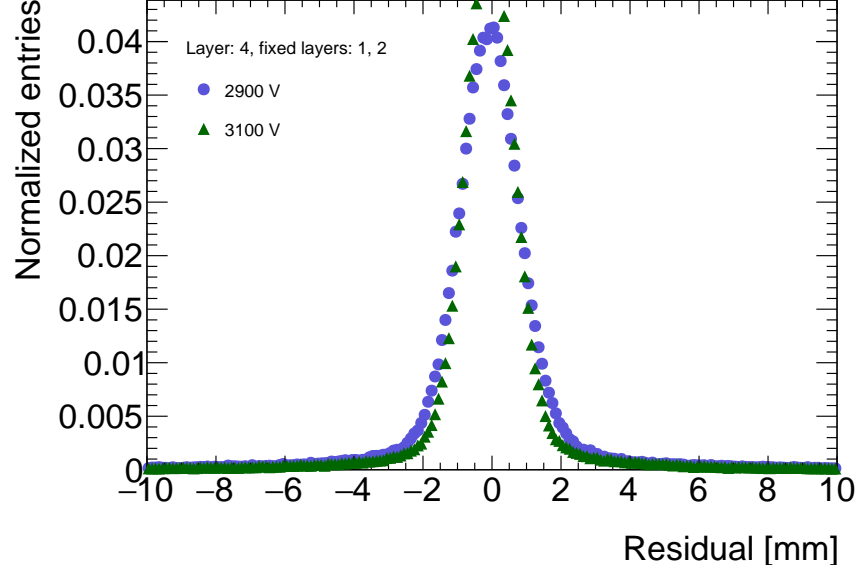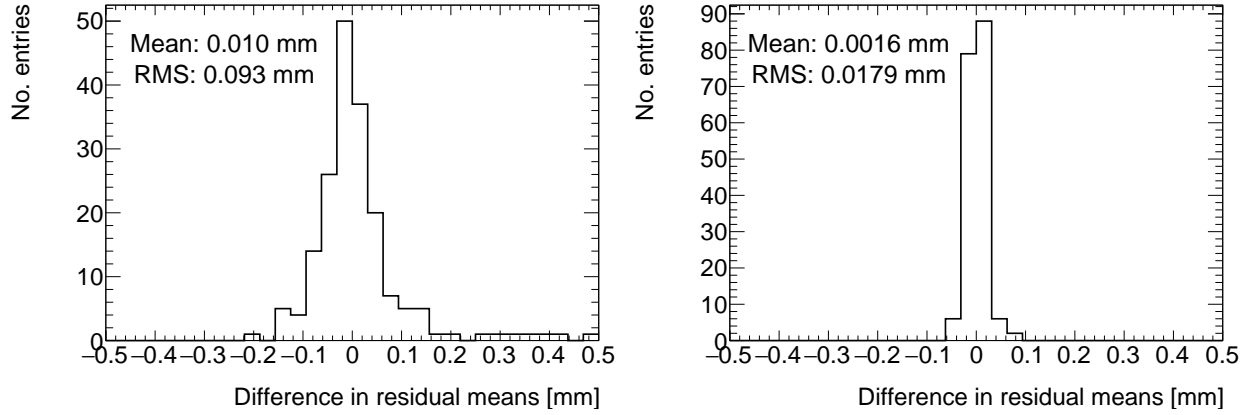
Figure C.3: Residual distribution for tracks on layer 4 built from hits on layers 1 and 2 for QL2.P.8 for data collected at 2.9 kV and 3.1 kV.

(a) Tracks on layer 4, reference layers 1 and 2.

(b) Tracks on layer 2, reference layers 1 and 3.

Figure C.4: Difference in residual means for data collected with QL2.P.8 at 2.9 kV and 3.1 kV respectively in 100 mm by 100 mm bins for (a) tracks on layer 4 built from hits on layers 1 and 2 and (b) tracks on layer 2 built from hits on layers 1 and 3.
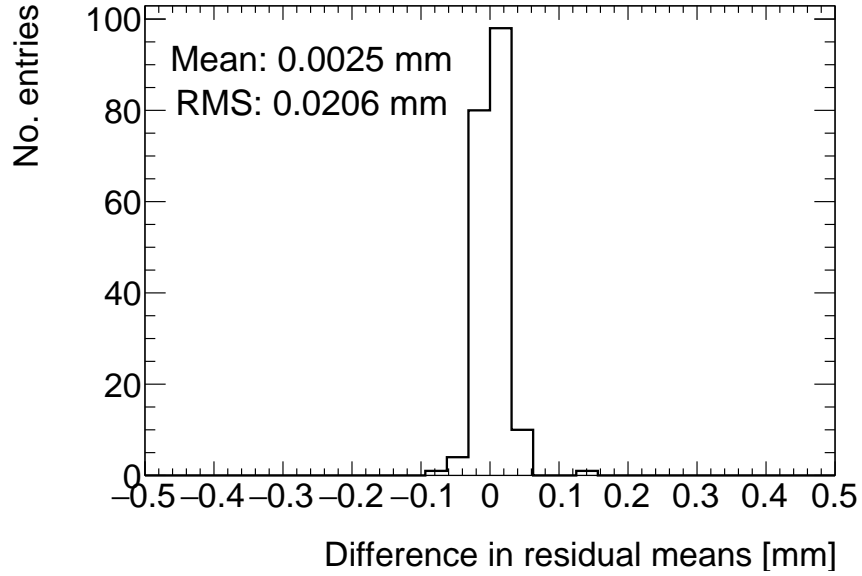
19

Figure C.5: Difference in residual means when the cluster fit algorithm is `Minuit2` [4] versus Guo's method [5] for tracks on layer 4 built from hits on layers 1 and 2 for QL2.P.8.

C.3   Cluster fit algorithm

To ensure that changing the cluster fitting algorithm like in appendix A would not change the calculated mean of residuals in each region of interest significantly, the residual means were compared in both cases. The distribution of the difference in residual means is plotted in figure C.5 for the tracking combination with the worst extrapolation lever arm.

The other tracking combinations had smaller RMS values. Differences on the order of 50 µm are important, so figure C.5 shows that the clustering algorithm had a small but notable effect. Therefore, the RMS for each tracking combination will be used to add a systematic uncertainty on the residual means.

C.4   OBSOLETE, DELETE LATER Area of residual distribution regions of interest

This section is outdated, and likely needs to be removed

20

The area of the region of interest in which to include tracks is primarily motivated by the misalignment model: the width of the region should be less than the scale on which the local offset is expected to change significantly. Changes in offset of order 50 µm, the approximate position resolution of the sTGCs in the η-coordinate, are significant. In a misalignment model with an offset and rotation, only the rotation changes the local offset with respect to the x-coordinate [1]. The distribution of the as-built cathode board rotation angles shows that the RMS of the rotation angle is 200 µrad [https://indico.cern.ch/event/1035057/ PG. 18]; however, the distribution has a long tail so a typical rotation angle of 1000 µrad was used here. A rotation of 1000 µrad will cause a 50 µm change in local offset over a change in x of 50 cm. Therefore, the width of the region of interest should be less than 500 mm.

Two other factors inform the width of the region. First, since the hits' x-coordinates are discrete the width in x must be larger than the pitch of the wire groups to ensure the bin will have a sufficient number of tracks fall in it. Second, more tracks will be included in a larger area so more statistics will be available for the residual distribution fit. For the bin widths wider than two wire groups, the statistics are sufficient. For each x-ray residual, the mean cosmics residual was calculated for a few different bin widths, and the difference in means plotted. Figure C.6 shows an example for QL2.C.4. The width of the distribution is on the order of 50 µm, showing that the calculation of the residual mean is relatively robust with respect to the area of the bin. However, 50 µm is greater than the typical statistical uncertainty on the cosmic residual of means, which ranges from 10 µm - 40 µm depending on the tracking combination under study. Therefore, the cosmic residual means are assigned an uncertainty of 50 µm.

For this analysis, 100 mm by 100 mm bins were used.

C.5 Differential non-linearity

In this context, differential non-linearity (DNL) is when the reconstructed cluster mean is biased by the fit of the discretely sampled PDO distribution over the strips. The bias depends on the relative position of the avalanche with respect to the center of the closest strip. For a summary of DNL, refer to page 40 of Lefebvre's thesis [1]. The cluster mean was corrected for DNL using the equation:

---

[1]The effect of rotation can be modeled by assuming the recorded track position is related to the hit position by a passive rotation. The angle of rotation is the relative angle between the layer of interest and the nominal geometry. The local offset does change with respect to the track's y coordinate as well, but negligibly in the limit of small rotation angles.
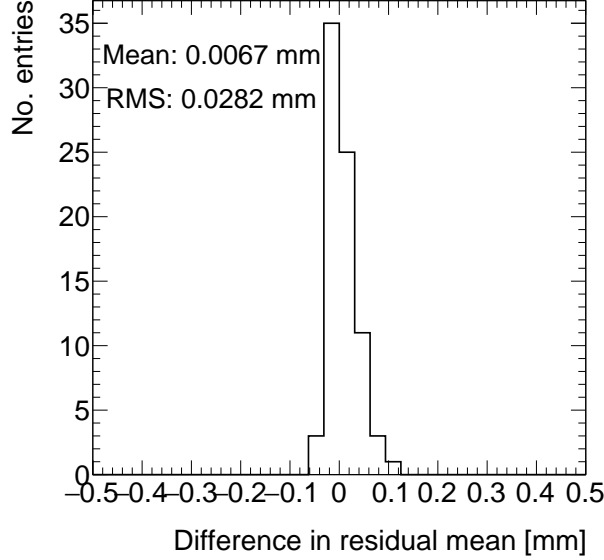
Figure C.6: Difference in cosmic residual means around x-ray residuals for square bins of 100 mm width and 200 mm width for QL2.C.4.

$$y' = y + a \sin\left(2\pi y_{rel}\right) \tag{C.2}$$

where y is the cluster mean, y_{rel} is the relative position of the cluster mean with respect to the strip's center, a is the amplitude of the correction, and y' is the corrected cluster mean. The amplitude can be derived by comparing the reconstructed hit position to the expected hit position, as done in Abusleme, 2016 [12]. With cosmic muons, there is no reference hit position to compare to, so track residuals were used as a proxy [1]. The hallmark of the DNL effect is the periodic pattern in the residual versus y_{rel} profile, and the effect of correcting the cluster means using an amplitude of $50\,\mu m$ is shown in figure C.7. An amplitude of $50\,\mu m$ was based on Lefebvre's estimate of the DNL amplitudes by layer, quadruplet and cluster size using exclusive cosmic muon tracks in `tgc_analysis/CosmicsAnalysis`. Little variation was seen in the amplitude parameters with respect to the quadruplet tested, the layer and the cluster size so a universal correction was used.

Although the correction is not large enough in this case, the figure shows that the correction does reduce the DNL effect. Slightly better performance is seen in the interpolation tracking combinations where the quality of the residuals is better. DNL corrections for cosmic muon data are difficult because the DNL effect is obscured by the effect of misalignments and
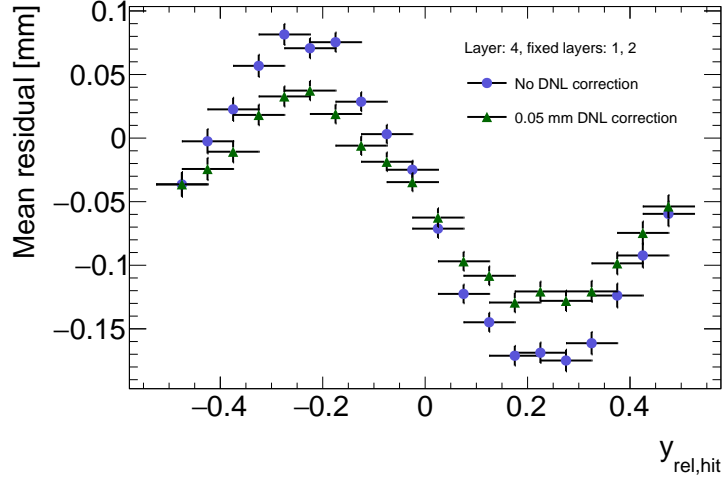
Figure C.7: Effect applying a $50\,\mu$m DNL correction to the cluster means on the residual vs y_{rel} distribution for tracks built from layers 1 and 2 and extrapolated to layer 4 for QL2.P.8.

noise. Misalignments cause the center of the sine pattern in figure C.7 to be shifted off of zero, since the mean of residuals is shifted.

In figure C.8, it is apparent that the effect of the DNL correction on the mean of the residual distribution in $100\,$mm by $100\,$mm areas is on the order of micrometers in the worst extrapolation case. Although the σ's of the residual distributions shrink with the DNL correction, the mean is the parameter of interest. Therefore, for this analysis DNL was not corrected for.

The σ's of the residual distributions do shrink with the DNL correction but not so much to affect the residual means, which are the important parameter for this analysis. Therefore, since the effect of the DNL correction is negligible, it was not pursued further.
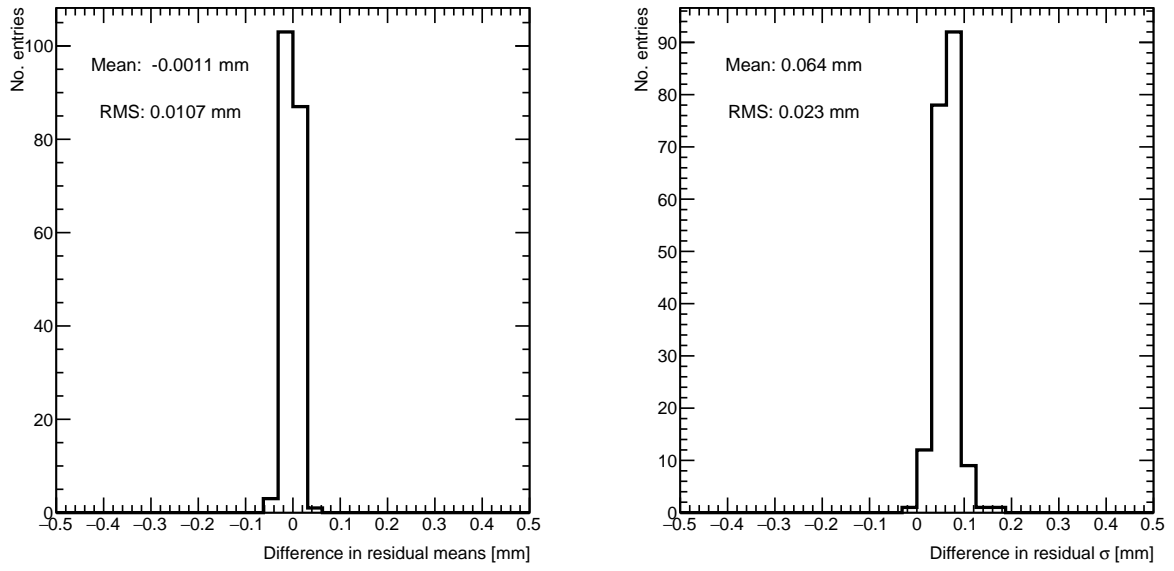
Figure C.8: Difference in residual distribution means and σ's with and without DNL correction for residuals on layer 4 from reference layers 1 and 2 for QL2.P.8.